metals

MDPI

Article

Influence of Flow-Gas Composition on Reaction Products of Thermally Treated NMC Battery Black Mass

Christin Stallmeister * and Bernd Friedrich

IME Process Metallurgy and Metal Recycling, Institute of RWTH Aachen University, Intzestr. 3, 52056 Aachen, Germany; bfriedrich@ime-aachen.de

* Correspondence: cstallmeister@ime-aachen.de

Abstract: The recycling of lithium-ion batteries (LIBs) is becoming increasingly important regarding the expansion of electromobility and aspects of raw material supply. Pre-treatment and liberation are crucial for a sufficient recovery of all relevant materials from LIBs. Organic removal and phase transformations by thermal pre-treatment are beneficial in many respects. This study deals with the influence of flow-gas composition on reaction products and water-based lithium recovery after thermal treatment. Therefore, a spent NMC black mass was thermally treated at 610 °C in a moved bed batch reactor under an N_2 atmosphere and mixtures of N_2 with 2.5% and 5% O_2. Since the phase transformation of the lithium content to Li_2CO_3 is targeted for water leaching, a treatment under a CO_2 atmosphere was studied as well. The resulting off-gas was analyzed by FTIR, and the black mass was characterized by XRD. Afterward, water washing of the black mass was carried out for selective lithium recovery. The gained lithium product was analyzed for the purity and phases present. The addition of O_2 resulted in reduced reduction reactions of lithium metal oxides and lower Li-yields in the water leaching compared to the other two atmospheres. In the case of CO_2, the formation of Li_2CO_3 is favored compared to LiF, but the Li-yield of 56% is comparable to N_2 treatment.

Keywords: lithium-ion battery; recycling; thermal treatment; pyrolysis; gasification; lithium; early-stage lithium recovery; water leaching; flow-gas composition

Citation: Stallmeister, C.; Friedrich, B. Influence of Flow-Gas Composition on Reaction Products of Thermally Treated NMC Battery Black Mass. *Metals* **2023**, *13*, 923. https://doi.org/10.3390/met13050923

Academic Editor: Antoni Roca

Received: 30 March 2023
Revised: 27 April 2023
Accepted: 6 May 2023
Published: 10 May 2023

1. Introduction

The ongoing electrification of our society leads to rising demands for energy storage systems. Therefore, LIB production is rapidly increasing. This leads to a high demand for battery raw materials such as cobalt, nickel, manganese, graphite, copper, and in particular lithium [1,2]. To ensure the availability of raw materials and, at the same time, meet the requirements of a circular economy, the recycling of used batteries and production scrap is essential [3]. Thermal pre-treatment of battery scrap before or after entering the first mechanical recycling steps offers several advantages, as described in the literature [4–10]. The main objective is the separation and evaporation of organics, originating from electrolytes, binders and separators [7,11]. In combination with the targeted phase transformation of the contained metal oxides [12], the thermal treatment process leads to the better leaching behavior of the black mass in the following hydrometallurgical steps [8,11] and allows for early-stage lithium recovery (ESLR) by a combination of thermal treatment and water leaching [5,9,13–20]. The thermal-induced phase transformation of the NMC cathode material enables the formation of water-soluble Li_2CO_3 as a reaction product. Afterward, the Li_2CO_3 can be recovered by the selective water leaching of the black mass fraction. This concept is promising since recycling lithium is challenging [5,9]. In common hydrometallurgical process routes, precipitation of lithium salts is the final step. Parts of the lithium are already lost in previous cementation and precipitation steps of the other battery metals [5,9]. In case of pyrometallurgical battery recycling, lithium is transferred to the slag phase [21–23] or flue dust [22,24–29]. This requires subsequent mechanical and hydrometallurgical processing of the slag for lithium recovery, which is energy and chemical intensive. With further

improvement, the reported concept of ESLR could overcome those drawbacks. Previous studies on spent NMC LIB shredders or black mass achieved lithium recovery yields of 60–64% after thermal treatment at around 600–700 °C [5,14,15,30]. Therefore, a deeper understanding of the process and the influence of its parameters on lithium recovery is necessary for process improvement.

The previous studies described below investigated the behavior of battery materials during pyrolysis under an inert atmosphere and incineration with air. Under an inert atmosphere, an increasing reduction in the contained NMC material with rising temperature was observed [12,16,17,30]. This leads to water-soluble Li_2CO_3 formation as a reaction product [14,15,30]. In contrast, Lombardo et al. found that after the incineration of NMC battery material with air, no reduction in the metal oxides could be observed in XRD analysis in the investigated temperature range from 450 to 650 °C [6]. Consequently, the ESLR process would not be promising in this case. Regarding organic removal and off-gas generation during incineration and pyrolysis, few studies are reported in the literature for different input materials. In the case of incineration of cathode materials, major products are reported to be CO_2, volatile hydrocarbons and H_2O [6,31]. In the case of incomplete combustion, as for the pyrolysis of whole battery cells, CO is detected as well [32]. Additionally, some studies deal with fluorine emissions [6,31,32], but no research was found regarding the influence of different oxygen concentrations in the flow-gas on off-gas and phase composition in the black mass.

In the case of CO_2 flow gas, to the best of the author's knowledge, not much has been reported in the literature to date. Park et al. [33] investigated the thermal treatment of pure NMC 811 and graphite mixtures under CO_2 and gained higher Li_2CO_3 recovery rates by water leaching compared to inert N_2 treatment. Schwich et al. [34] reported a leaching efficiency of 60% for thermally treated NMC black mass under a CO_2 atmosphere, but without focus on the behavior or influence of CO_2 during the thermal treatment compared to other flow-gas compositions. For a better understanding of the process and in order to develop further optimization options for thermal treatment, the present study investigates the influence of different flow-gas compositions on both the off-gas and the black mass achieved, as well as the effects on the ESLR process. An inert N_2 atmosphere, with mixtures of N_2 with up to 5% O_2, and a pure CO_2 atmosphere are investigated comparatively at 610 °C. The trials were carried out in an oscillating tube furnace to ensure maximized solid–gas contact between black mass and flow-gas. The maximum tolerable O_2 amount in the process atmosphere to ensure the conversion of Li to Li_2CO_3 as completely as possible is to be identified within this work for the first time. Information in this regard is also of interest for plant engineering and construction. Additionally, the promising results of Park et al. [33], who gained higher Li recovery yields by thermal treatment under a CO_2 atmosphere compared to N_2 from a mixture of pure NMC 811 and graphite, are transferred and investigated for an end-of-life battery black mass containing further potential interfering elements, such as fluorine. Since the process is carried out in a moved bed reactor with enhanced solid–gas interaction, higher Li_2CO_3 yields are expected compared to previous studies with CO_2 addition. The addition of O_2 to the process suggests increased CO_2 formation in the exhaust gas due to combustion reactions as well. Accordingly, in this study it is to be evaluated whether the oxidation behavior of the NMC oxides, or the favored formation of Li_2CO_3 under CO_2 atmospheres expected from the literature [33,34], prevails as a function of the O_2 addition. To assess carbonate formation in the context of the thermal pre-treatment of battery materials, this study is the first, to the authors' knowledge, to determine the inorganic carbon content after water leaching.

2. Materials and Methods

The input feed for the thermal treatment trials was an NMC 622 LIB black mass generated from an industrially inert shredder process under an N_2 atmosphere, followed by drying below 80 °C. Separation of the black mass from the shredded material was carried

out by sieving at 0.5 mm at TU Freiberg. Table 1 provides the chemical composition of the black mass fraction, analyzed by the ICP-OES (Spectro CIROS Vision, Spectro Analytical Instruments GmbH, Kleve, Germany) combustion method for carbon analysis (ELTRA CS 2000, ELTRA GmbH, Haan, Germany) and ion chromatography (811 Compact IC pro, Deutsche Metrohm GmbH & Co. KG, Filderstadt, Germany).

Table 1. Chemical composition of the black mass.

Element	Al	Cu	Co	Li	Mn	Ni	P	C	F
wt.%	2.02	1.83	5.30	3.21	5.09	14.6	0.55	39.90	2.50

The thermal treatment trials were conducted in an oscillating quartz-tube furnace (TSO 11/400, Carbolite Gero GmbH & Co. KG, Neuhausen, Germany). Therefore, 80 g active mass per trial, and 100 g in case of CO_2 treatment, was fed into the quartz tube. The material was heated up simultaneously with the furnace with a heating rate of 300 °C/h to 610 °C, followed by a 1 h holding time. The temperature was measured in the center of the tube with a type-N thermocouple. The tube was oscillating during the trial in a range of 315 ° and a frequency of 7 full oscillations per minute. During the heating and holding time, the different investigated flow-gas compositions were inserted with a flow rate of 4 L/min:

- N_2 (trials in triplicate);
- N_2 + 2.5% O_2 (trials in duplicate);
- N_2 + 5% O_2 (trials in duplicate);
- CO_2 (trials in duplicate).

After the holding time, the heating power was turned off, and the flow-gas was switched to N_2. Oscillation and N_2 gas flow were turned off when the temperature dropped below approx. 200 °C. The resulting off-gas, except for the trials under a CO_2 atmosphere, was continuously analyzed by an FTIR (CX4000 FTIR gas analyzer, Gasmet Technologies Oy, Vantaa, Finland) and additional O_2 (Oxygen Analyzer PMA 10, M&C TechGroup, Ratingen, Germany) and H_2 (CONTHOS 3—TCD, LFE GmbH & Co. KG, Bruchköbel, Germany) measuring units for its composition. For exhaust cleaning, the gas flowed through a two-stage scrubbing unit first with NaOH solution and second with water, followed by a catalytic post-combustion. The <90 µm fraction of the thermally treated black mass was analyzed by XRD (MiniFlex, 40 kC, Cu-tube, Rigaku) and SEM EDX (S3700N Hitachi, Quantax 200 detector, 123 eV MnKalpha).

After thermal treatment, water leaching of 20 g black mass per trial was carried out with 500 mL deionized water in a glass backer. The solution was stirred for 90 min at room temperature at 200 rpm. During subsequent filtration, the filter cake was washed with 200 mL of deionized water and afterward dried at 80 °C for 24 h. The filtrate was analyzed for Li, Al and P by ICP-OES and by TOC analyzer for organic and inorganic carbon in solution (multi N/C 2100/2100S, Analytik Jena GmbH, Jena, Germany). Fluorine determination was carried out by ion-selective electrodes (Methrom Titrando 888, Deutsche Methrom GmbH & Co. KG, Filderstadt, Germany). Analysis of the filter cake was carried out similarly to the input material for the elements Li, Al, F, P and C.

The filtrate was vaporized by boiling the solution to recover a lithium salt product. The purity and phase composition of residual salt were analyzed by ICP-OES, combustion method, IC and XRD, similar to the previous samples. The whole process is summarized in Figure 1.

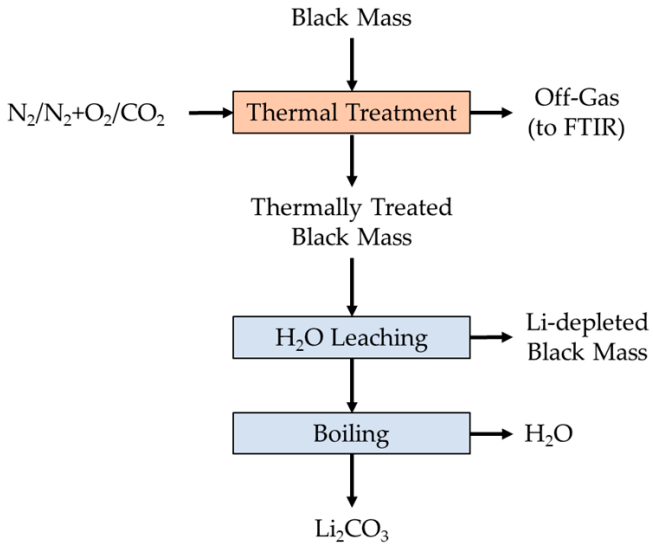

Figure 1. Process schema of this study.

3. Results and Discussion

The following sections provide the results of the thermal treatment trials, including off-gas and black mass characterization, as well as the outcomes of water-leaching trials with the different thermally treated black masses.

3.1. Off-Gas Analysis

The analysis of resulting off-gas from the pyrolysis trials was carried out for a deeper understanding of the influence of different oxygen partial pressures in the flow-gas on the ongoing reactions during the process. In general, several different gases were detected, such as CO, CO_2, H_2O; hydrocarbons; other organics such as alcohols and aromatic compounds; electrolyte compounds EC, DMC, DEC, EMC and HF; and POF_3 emissions, as shown in Figure 2.

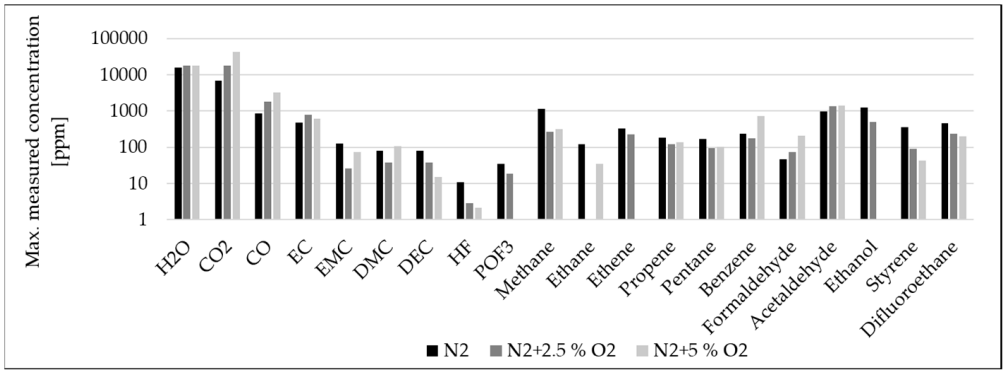

Figure 2. Detected gases with their max. concentration, plotted in logarithmic scale.

Because of this complex off-gas composition, exact analysis is challenging and limited. During some trial periods, the gas is highly concentrated, which results, together with interferences/overlaps of different compounds, in high intensities of the measured spectrums. This, in turn, leads to inaccuracies in the measured component concentrations. Moreover, not all evaporating gases can be identified due to a leak of reference data. This could be the case, e.g., for some fluorinated hydrocarbons, reported to originate from PVDF decomposition [35]. Nevertheless, the presence of the addressed gases can be determined, but with inaccuracies of the measured concentrations. However, the qualitative curve progression

and their comparison within the different trials is possible and provides information about different ongoing reactions as regards their dependence on the oxygen partial pressure.

The comparison of CO_2 and CO generation during the trials between the different oxygen partial pressures, presented in Figure 3, shows similar minima and maxima and temperature timings but different amounts of gas release. At around 150 °C, the first peak of CO_2 generation is detectable with comparable concentration between all trials. It is attributed to the decomposition of the conducting salt and the solid electrolyte interface, according to Equation (1) [32,36].

$$(CH_2OCO_2Li)_2 \rightarrow Li_2CO_3 + C_2H_4 + CO_2 + \frac{1}{2}O_2. \quad (1)$$

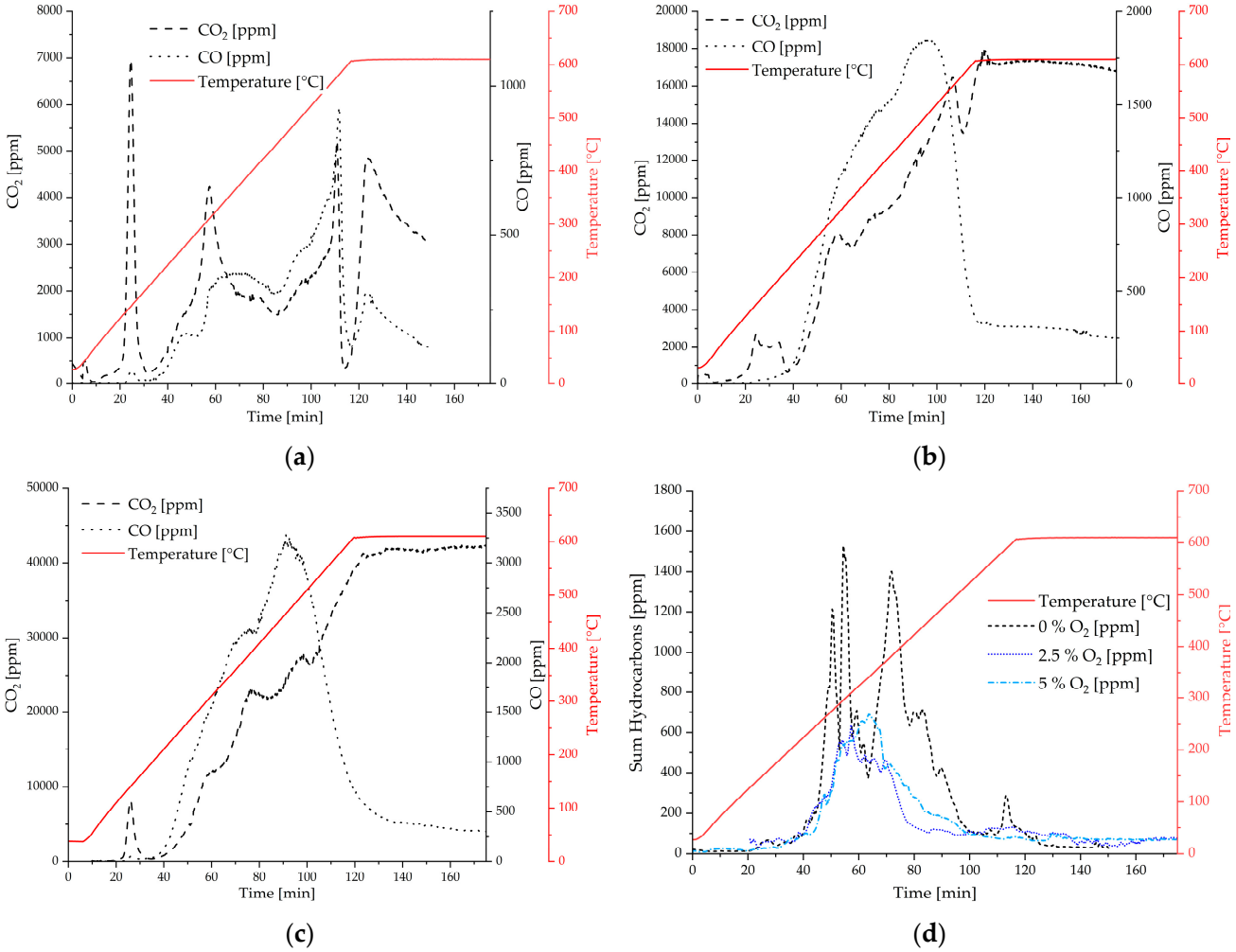

Figure 3. CO_2 and CO release during the thermal treatment under (**a**) N_2; (**b**) N_2 + 2.5%O_2; (**c**) N_2 + 5% O_2 atmosphere and (**d**) comparison of release of hydrocarbons between different O_2 concentrations.

The second peak of CO_2 release occurs at approx. 300 °C but differs in the concentration of CO_2 by the factor of 1.9 (N_2 vs. 2.5% O_2) and 2.8 (N_2 vs. 5% O_2). Further characteristic peaks and plateaus are detectable at around 400 °C and 500 °C and within the start of the holding time at 610 °C. The difference in CO_2 concentration is also rising with temperature; e.g., for the third CO_2 peak at 400 °C, the factors are 3.4 (N_2 vs. 2.5% O_2) and 8.1 (N_2 vs. 5% O_2). The peaks are attributed to the organic decomposition from the battery material. The main electrolyte compound of the investigated material is EC, with a boiling temperature of 248 °C [37]. Therefore, its release and also decomposition is

detected from this temperature. Between 400 and 500 °C, the decomposition of separators and binders takes place [31]. Because the detectable peaks during the gas release occur at similar temperatures for all considered atmospheres, it can be concluded that the decomposition temperatures of the organic compounds are not shifted. Therefore, to reach complete organic removal, the same maximum temperature is necessary. In the tests with 0% and 2.5% O_2, an anomaly occurs in the gas measurement at the hold time onset. There is a short but strong drop in concentration followed by a rapid increase. This drop is due to a brief interruption of the gas supply by the furnace control unit and not due to chemical reactions.

In the case of CO, the qualitative curve progression is similar between the trials but differs in quantitative results as well. In general, higher O_2 partial pressure results in higher amounts of released combustion products: CO_2 and CO. As a result, lower hydrocarbon concentrations are detected, as presented in Figure 3d. The shape of the curves differs between the trials, so the maxima of hydrocarbons occur at different temperatures for different O_2 concentrations. In particular, the components CH_4 and C_2H_4, which make up the largest share, occur in lower concentrations due to the partial combustion resulting in CO_2, CO and H_2O, according to Equations (2) and (3) [38].

$$C_xH_y + \left(x + \frac{y}{4}\right)O_2 \rightarrow xCO_2 + \frac{y}{2}H_2O \quad (2)$$

$$C_xH_y + \left(\frac{x}{2}\right)O_2 \rightarrow xCO + \frac{y}{2}H_2O \quad (3)$$

The three maxima of hydrocarbon release under an inert atmosphere, attributed to the different phases of pyrolysis processes, as described and discussed in another study by the authors [30], are not present in the case of O_2 addition. With rising temperature, the combustion reactions are favored. The reactions of O_2 with solid carbon take place during the holding time since the CO_2 concentration remains at a high level during the holding time, even though no further hydrocarbons are released in this temperature range, also in an inert atmosphere. This is confirmed by the XRD characterization of the black mass in Section 3.2, but it cannot be identified if the CO_2 is a reaction product from the combustion of formed pyrolysis coke or graphite. The decreasing CO_2 concentration over the holding time under an inert atmosphere indicates the termination of both organic decomposition and reduction reactions of metal oxides.

Regarding HF release, a general correlation between HF concentration and O_2 partial pressure can be derived from the FTIR analysis: With increasing O_2 addition, the HF concentration in the off-gas decreases (see Figure 2). Diaz et al. [32] found a similar correlation by comparing treatment under air and N_2. However, since the total off-gas volume could not be measured in the present study, it cannot be determined whether total HF emission is lower or if its concentration is diluted.

3.2. Black Mass Characterization

Characterization of the produced black mass by SEM-EDX and XRD measurement allows for further conclusions regarding chemical reactions during thermal treatment. The comparison of SEM images between untreated and black mass treated with different oxygen concentrations, presented in Figure 4, indicates structural changes regarding the NMC particles.

NMC particles (bright, light grey) from thermally treated samples look more spending than those untreated, especially with increasing O_2 content during thermal treatment. The shadows around the individual particles caused by the binder [39] are also reduced by thermal treatment, particularly by the addition of O_2. However, binder residuals around the NMC particles can be detected in all samples. Whether the approx. 10 µm large NMC particles have decomposed to smaller particles due to the thermal treatment cannot be accurately estimated from the SEM images.

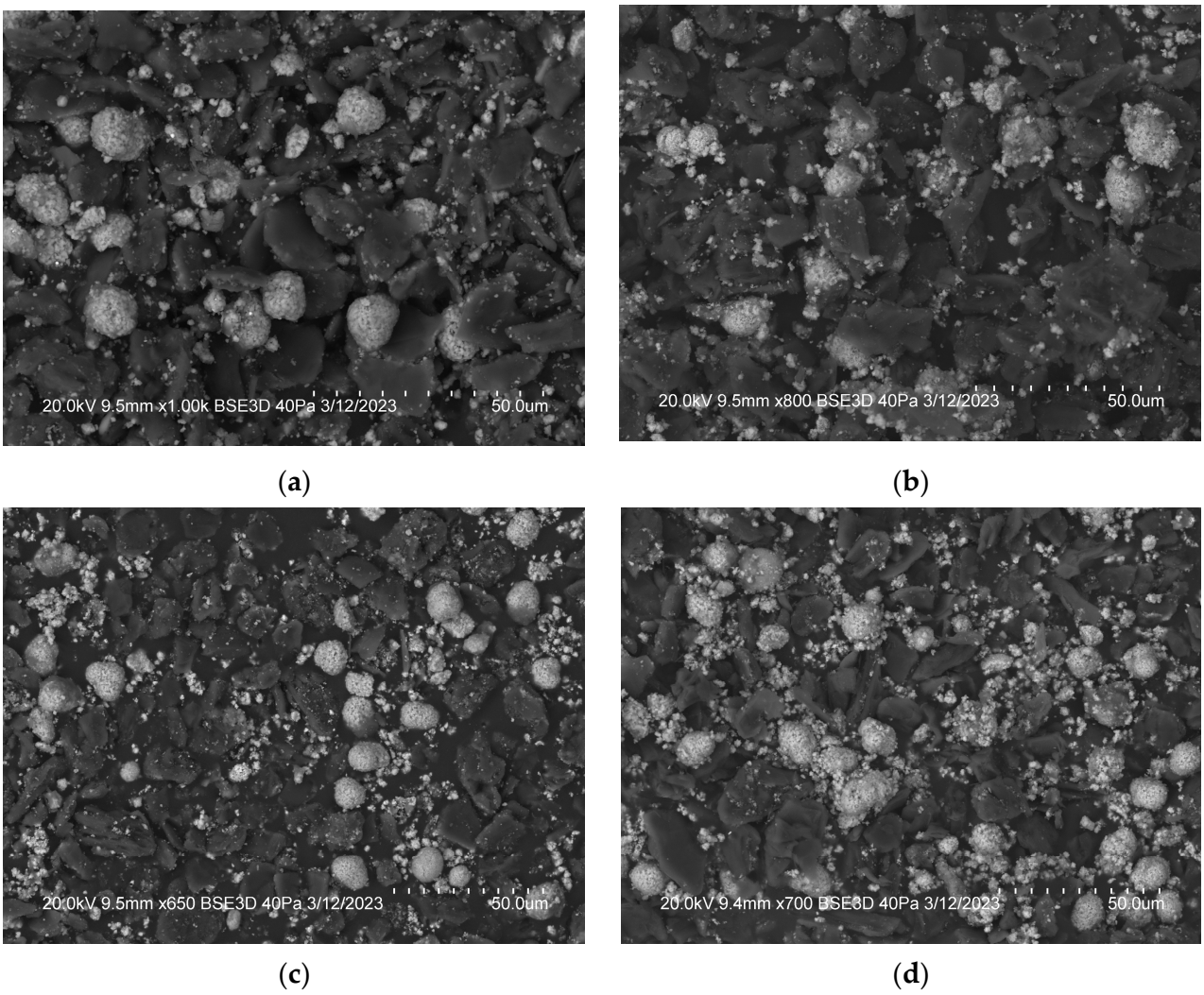

Figure 4. SEM images of (**a**) untreated black mass and black mass treated under (**b**) N_2; (**c**) N_2 + 2.5% O_2; (**d**) N_2 + 5%.

In all samples, Al can be detected by EDX-spot analysis on the NMC particles in shares of 1.5–6 wt.%. Since the black mass originates from NMC 622 cells, this indicates an alumina coating of the particles, as reported in the literature [40,41].

In the case of thermal treatment under a CO_2 atmosphere, black mass particles, presented in Figure 5, look similar to inert treated material, with binder residues detectable around NMC particles. In contrast to the other SEM images, aluminum content, measured by EDX-spot analysis, is higher. Elemental analysis of the large particle in the lower right corner of the image provides an Al share of 94 wt.%. Its origin cannot be identified, but the partial smelting and oxidation of aluminum foil or the agglomeration and sintering of single particles could be possible explanations.

The XRD analysis with HighScore [42] of the different treated black masses, given in Figure 6, shows different phases depending on the flow-gas composition during thermal treatment. In the case of inert treatment under N_2, the lithium-nickel-manganese-cobalt-oxides (LNMCO) from the untreated black mass are no longer detectable. They were reduced to NiO, metallic Ni, according to the exemplary reactions (4)–(7) derived from [12,43], and, in contrast to a previous study with a whole battery shredder in a fixed-bed reactor [30], to LCO. Since reflexes of different metal oxides (e.g., MnO, NiO, CoO) overlap, they cannot be clearly distinguished in the XRD pattern, but their existence is assumed. Another product of the reduction is Li_2CO_3 (see Equation (8), the reflexes of which are identified. In contrast,

with the addition of O_2 during thermal treatment, Li_2CO_3 is not detectable by XRD. The lithium metal oxides are less reduced with rising O_2 concentration so that LMNO, LMO and LCO are still present in the black mass, and with 5% O_2, no metallic Ni is detectable. Investigations of Lombardo et al. [6,44] concluded that incineration under air results in no change in the phase composition of the black mass compared to the untreated sample with respect to the cathode material. The present study shows additionally that 2.5% O_2 already inhibits the reduction reactions but not to the same extent as incineration under air. Potential reaction partners such as hydrocarbons are no longer available to the same extent due to combustion reactions. Moreover, a comparison of the intensity of graphite reflexes between the different O_2 concentrations indicates the partial combustion of it by O_2 addition. This is confirmed by CO_2 formation during the holding time of the experiments, described in Section 3.1.

$$8CH_4 + LiNiO_2 \rightarrow CO_2 + 4Li_2O + 8NiO + 2H_2O \quad (4)$$

$$2LiNiO_2 + CO \rightarrow CO_2 + Li_2O + 2NiO \quad (5)$$

$$4LiNiO_2 + C \rightarrow CO_2 + 2Li_2O + 4NiO \quad (6)$$

$$NiO + CO \rightarrow CO_2 + Ni \quad (7)$$

$$3Li_2O + 3CO_2 \rightarrow 3Li_2CO_3 \quad (8)$$

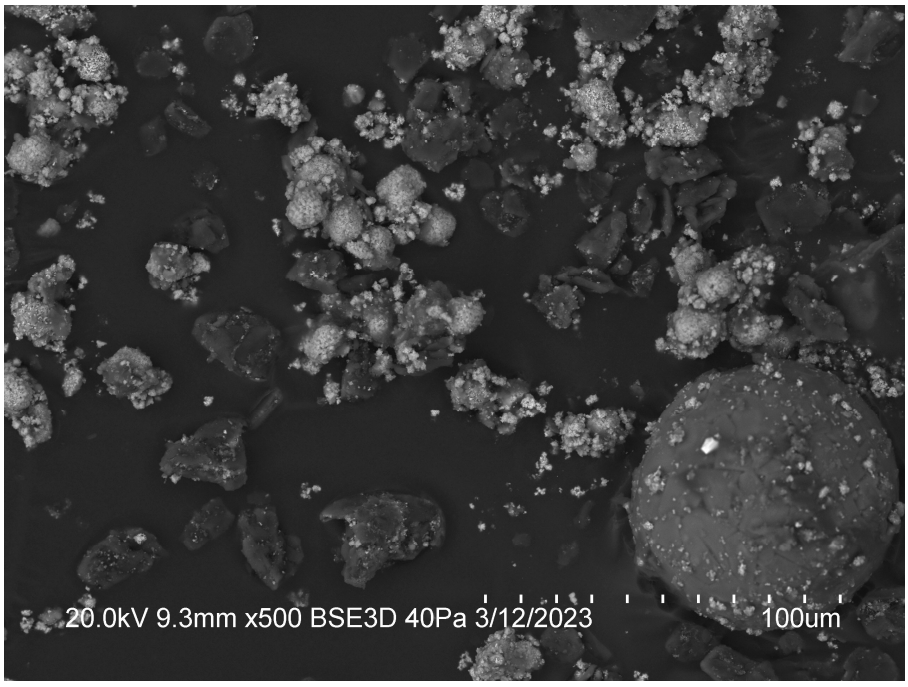

Figure 5. SEM image of black mass thermally treated under a CO_2 atmosphere.

In the case of thermal treatment under a CO_2 atmosphere, LNMCO is decomposed to LCO, LMCO and metallic Ni. Similar to inert N_2 treatment, targeted Li_2CO_3 is identified in the XRD pattern, but since LMCO is detectable in contrast to the inert-treated sample, a weaker reduction is assumed. In the literature, favored CO production due to the Boudouard reaction under a CO_2 atmosphere at 600 °C in the presence of graphite was

reported [33]. Due to verifiable LMCO and LCO content in the sample, it is more likely that in the case of organics containing EoL black mass, the thermochemical equilibrium of organic cracking with a CO_2 product (see Section 3.1) is shifted and results in a more endothermic process than under an inert atmosphere. Therefore, decomposition reactions could be hindered. This explanation will be further investigated in following studies.

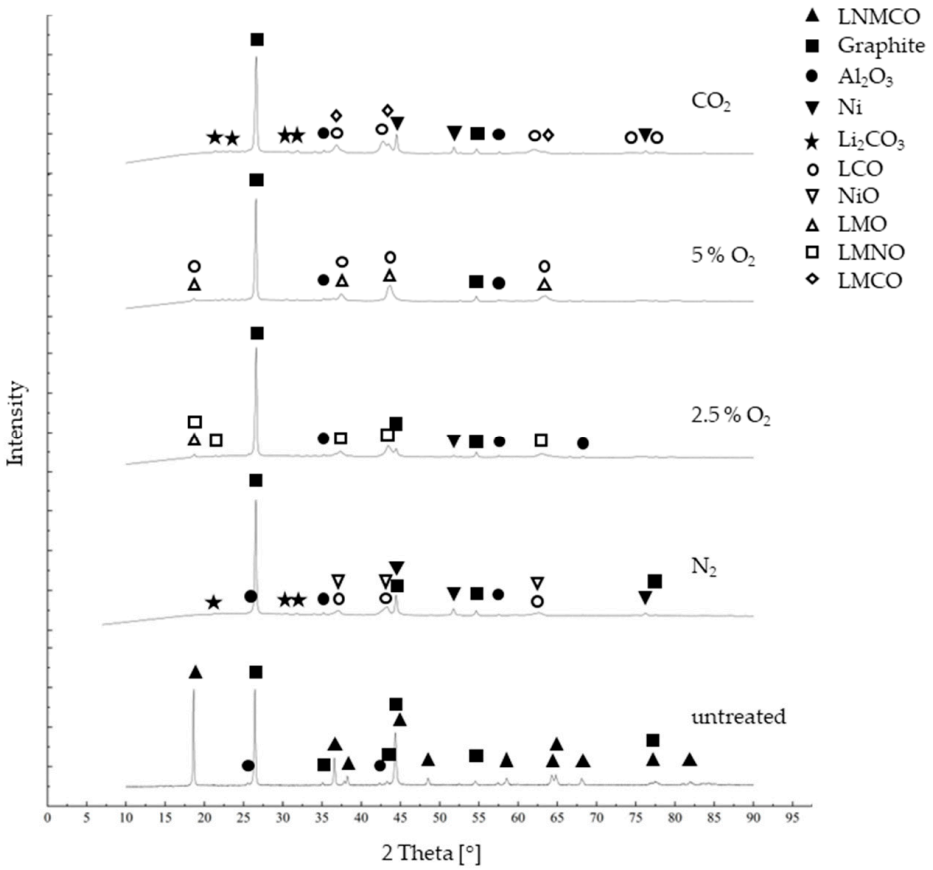

Figure 6. XRD analysis of untreated and different thermally treated black mass.

3.3. Water Leaching

Water-leaching trials were carried out to recover lithium from the black mass and obtain an enhanced understanding of the reactions taking place during the thermal treatment. Therefore, leaching efficiencies of Li, Al and F were calculated based on Equation (9).

$$LE_{x_i} = \frac{x_i \text{ in solution [g]}}{x_i \text{ in solution [g]} + x_i \text{ in filtercake [g]}} \cdot 100\% \quad (9)$$

$$LE: \text{ leaching efficiency; } x_i: \text{ Considered Element(Li; F; Al)}$$

The resulting leaching efficiencies for Li are presented in Figure 6. As expected from previous research [30] and the literature [14,15], inert thermal treatment results in better Li leaching efficiency than from untreated black mass due to the described reductive reactions of lithium metal oxides in Section 3.2. From untreated material, 13.5% of Li is recovered by water leaching. The leaching efficiency is increased to 55.7% by inert thermal treatment, which is lower than the 62% obtained in previous research with a complete shredder fraction [30] or other studies from the literature with coated foil fractions and separators [14]. This could be explained by the lower organic content of black mass compared to the whole shredder fraction; e.g., Rouquette et al. [14] found a positive impact of the presence of a separator material during thermal treatment on Li recovery by water leaching. When

treating a black mass fraction without a separator under an inert atmosphere, they reached an Li recovery of 35% after water leaching, compared to 61% in the case of separator addition [14]. The Li recovery rate in this study is located between those two values, which is probably due to the different organic contents of the input materials. This will be further investigated in following studies.

The comparison of Li leaching efficiency between samples from N_2 and N_2 + O_2 atmosphere treatments shows a negative impact of O_2 addition during thermal treatment on Li recovery by water leaching (see Figure 7). The described inhibited reduction reactions of lithium metal oxides described in the previous chapters result in less formation of water-soluble Li_2CO_3. For this reason, the leaching efficiency decreased from 55.7% to 36.6% and 27.4%. The decrease in inorganic carbon concentration in the solution with rising O_2 addition during thermal treatment confirms this explanation.

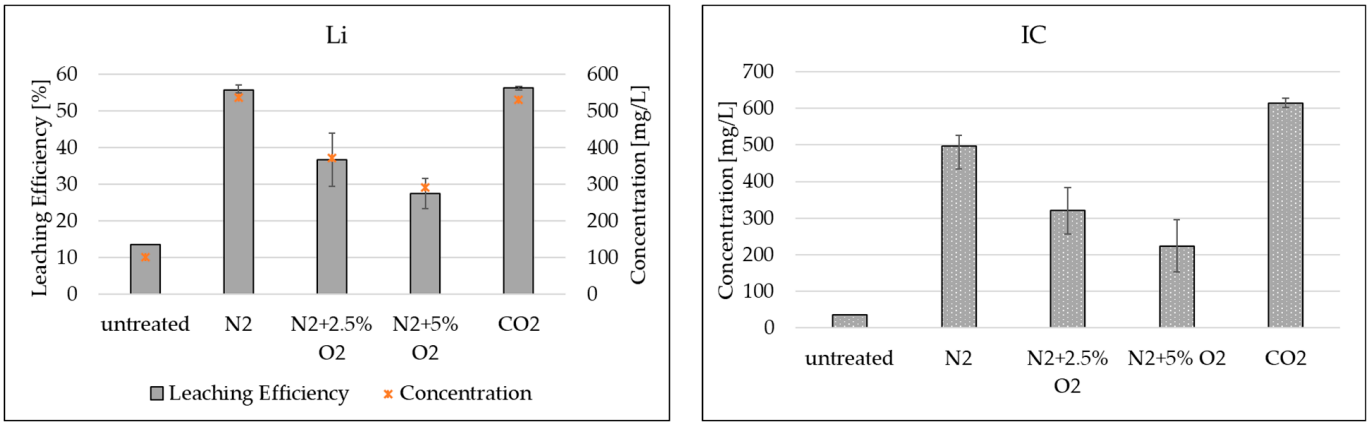

(**a**) (**b**)

Figure 7. Leaching efficiency and concentration of (**a**) lithium and (**b**) inorganic carbon concentration in solution in dependence of thermal treatment parameters.

In the case of thermal treatment under a CO_2 atmosphere, the Li leaching efficiency of 56.2% is similar to the results of N_2 treatment. However, the amount of dissolved inorganic carbon in the solution is 614.5 mg/L and higher than for N_2 treatment with 497.3 mg/L. This allows for the conclusion of higher dissolved carbonate salt amounts. The comparison with the behavior of fluorine leachability, shown in Figure 8, supports this explanation: The leaching efficiency of F, as well as the F concentration in solution, is lower for black mass from CO_2 thermal treatment than from pyrolysis under N_2. This could be due to a more preferential formation of Li_2CO_3 instead of LiF, because of the shift of the equilibrium of reaction (10) [45,46] during thermal treatment under a CO_2 atmosphere. Fluorine leaching efficiency is also lower for black mass from thermal treatment with O_2 addition compared to N_2 treatment. A decreased reduction in lithium metal oxides results in less Li_2CO_3 formation and therefore the reduced possibility of a reaction of Li_2CO_3 with released HF, according to Equation (10).

$$Li_2CO_3 + 2HF \rightarrow 2LiF + CO_2 + H_2O \quad (10)$$

Moreover, as described in Section 3.1, HF concentration in the off-gas lowers with rising O_2 addition, resulting in the decreased reaction activity of HF.

Besides F, Al is the main impurity in the water-leaching process. The co-leaching behavior is presented in Figure 8. In the case of the untreated material, the leaching efficiency of Al is 0.3%. It rises to 4.5% and up to 6.3% for N_2 and N_2 + O_2 treatment. Between the black masses from thermal treatments under different N2 + O_2 mixtures, no coherence of Al leaching efficiency can be derived. In contrast, thermal treatment under CO_2 leads to higher leaching efficiencies of Al. This can be attributed to the higher pH

value of the solution due to the larger amount of Li_2CO_3 that causes Al corrosion as derived from the Pourbaix diagram of Al [47]. Although the formation of AlF_3 is possible during pyrolysis [15,46], the increased solubility of this salt is not assumed due to the lower F content in the solution compared to N_2 trials.

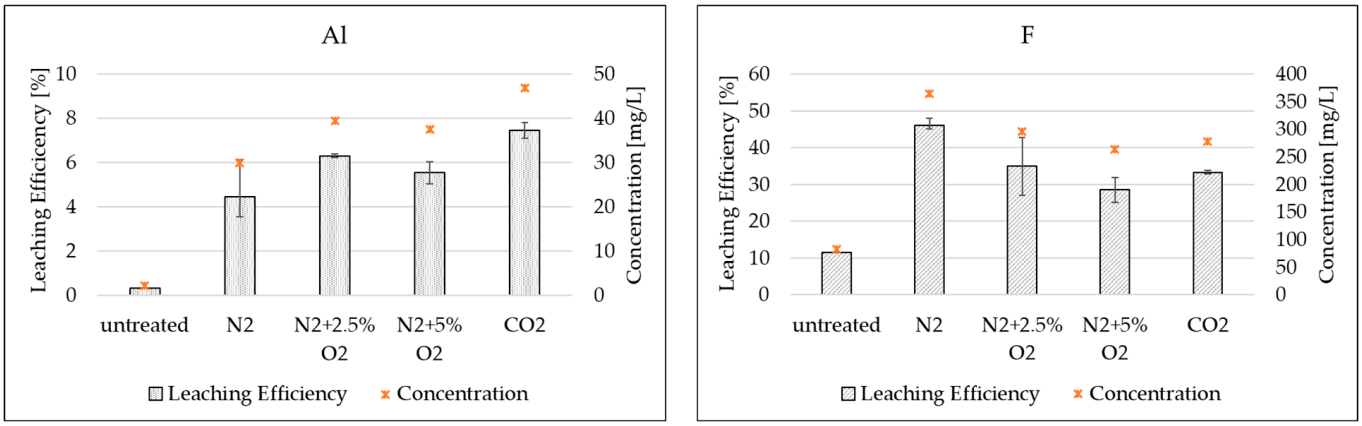

(**a**) (**b**)

Figure 8. (**a**) Al and (**b**) F leaching efficiencies and concentration in dependence of thermal treatment parameters.

After leaching, the precipitation of the lithium salt product was carried out by the complete evaporation of water by boiling. An additional XRD analysis of the generated salts, presented in Figure 9, confirms the described relationships between Li, F and IC analysis. All samples mainly consist of Li_2CO_3 and LiF, with dominating carbonate reflexes. As expected from the leaching results and black mass analysis, the semi-quantitative carbonate shares of the samples originating from treatment with O_2 addition are lower than for N_2 and CO_2 treatment. In addition, unidentifiable phases occur in the two samples with O_2 addition. Therefore, the given LiF and Li_2CO_3 shares are semi-quantitative and normalized values. In the case of CO_2 thermal treatment, the largest share of Li_2CO_3 was achieved, as expected from the IC and F analysis in solution. The Al impurities are not detectable in XRD analysis due to low concentrations.

The elemental impurity concentrations of the salts were determined for the two process parameters with the best lithium leaching efficiencies (N_2 and CO_2 thermal treatment). The averaged values of the retries are given in Table 2.

Table 2. Elemental concentration of impurities in Li salts.

Atmosphere	Al	F	P	Mn	Ni	Co	Cu
		wt.%			ppm		
N_2	1.00 ± 0.26	9.99 ± 0.21	0.20 ± 0.02	59	110 ± 29	89 ± 34	<50
CO_2	1.47 ± 0.03	7.22 ± 0.28	0.09 ± 0.003	<50	71 ± 5	54 ± 4	<50

The main impurities in the Li salt are Al and F. The described different leaching behaviors of Al and F for different pre-treatment atmospheres is confirmed. The Al content in the salt generated from the thermally treated black mass under an N_2 atmosphere is lower, but therefore F content is higher. Cu and Mn content were, except for one sample, below the verification limit of ICP-OES. Ni and Co impurities of 54–110 ppm were detected but may originate from small particles that have not been filtered when separating the black mass fraction from the leach solution, since the metal oxides are not soluble in water [48]. Although Co can be dissolved in the basic environment, Ni cannot [46], and their co-leaching has not yet been reported in the literature. Nevertheless, no pure Li_2CO_3

product is generated, so the further processing of the product or adjustment of the leaching parameters is necessary in future studies, as described in the literature as well [14].

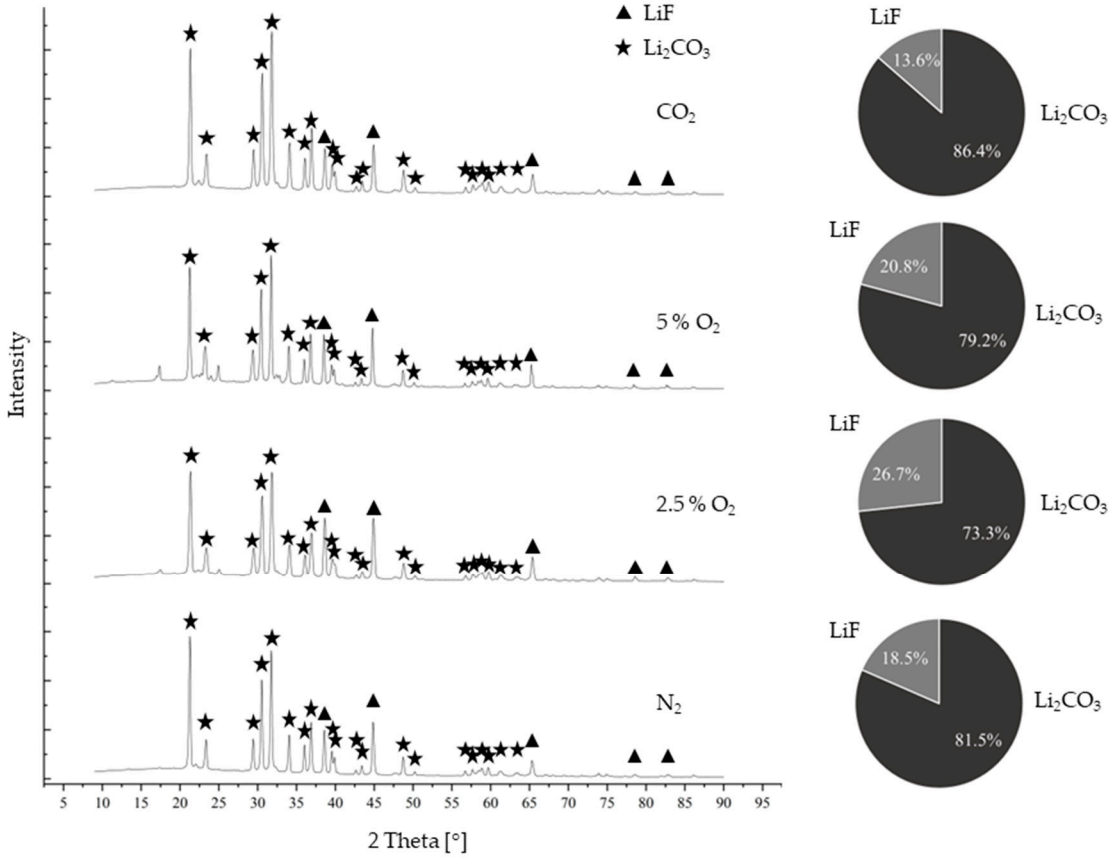

Figure 9. XRD analysis of recovered Li salts with semi-quantitative Li_2CO_3 and LiF share, normalized and calculated by Reference Intensity Ratio method.

The presented results show a significant influence of the selected gas atmosphere on the products of the thermal treatment and, in particular, on lithium recovery. Based on the results, CO_2 is considered as the favored atmosphere regarding targeted Li_2CO_3 formation. The suppressed formation of LiF leads to reduced F impurities in the Li salt product. Although the Al impurity increases, this is also to be expected with further Li yield increases due to the basic pH value of the solution. Since even low O_2 concentrations of 2.5% lead to a decreased reduction in the NMC oxides, an O_2-free atmosphere should be preferred in case of water-based Li recovery. Future studies will focus on a more complete reduction in the NMC oxides and the prevention of side reactions of Li with other battery elements.

4. Conclusions

The influence of different flow-gas compositions in thermal treatment processes of spent NMC black mass on the gaseous and solid products and the following water-based lithium recovery step were investigated in this study. The addition of O_2 to the flow-gas leads to the partial combustion of organics contained in the black mass by generating higher CO_2 and CO concentrations in the off-gas. Their concentrations increase with increasing O_2 addition. In this context, the concentration of hydrocarbons decreases.

Regarding the black mass products, rising O_2 addition and the changed off-gas composition lead to less reduction reactions of lithium metal oxides in the black mass, compared to inert N_2 treatment. In contrast to the combustion under air described in the literature [46], reduction reactions still take place in the investigated concentration range of O_2 addition

but are incomplete even for the lowest investigated O_2 addition of 2.5%. This has a significant influence on the water-leachability of contained lithium since the transformation to Li_2CO_3 is dependent on the reduction reactions. Therefore, the leaching efficiency of lithium is decreased from 55.7% to 36.6% (2.5%O_2) and 27.4% (5%O_2).

Thermal treatment under a CO_2 atmosphere resulted, according to XRD analysis, in less complete lithium metal oxide decomposition and a more endothermic process compared to N_2 treatment, but similar Li leaching efficiency of 56.2% in the water-leaching step. A difference is the higher and beneficial IC content in solution as well as the lower leaching efficiency of F compared to N_2-treated material. The assumed suppression of LiF formation needs to be investigated in follow-up studies. Since Li_2CO_3 formation is favored for Li recovery, a CO_2 atmosphere offers a high potential to condition the LIB material for subsequent metal recovery. To further enhance the Li recovery, a follow up study is planned with whole LIBs shredder fractions and parameter adjustment to create the most reducing conditions as possible.

Author Contributions: Conceptualization, C.S.; methodology, C.S.; validation, C.S.; formal analysis, C.S.; investigation, C.S.; resources, C.S.; data curation, C.S.; writing—original draft preparation, C.S.; writing—review and editing, C.S. and B.F.; visualization, C.S.; supervision, B.F.; project administration, C.S.; funding acquisition, C.S. and B.F. All authors have read and agreed to the published version of the manuscript.

Funding: This research was funded by the German Federal Ministry of Education and Research (BMBF), in the frame of the project "InnoRec", grant number 03XP0246D.

Institutional Review Board Statement: Not applicable.

Informed Consent Statement: Not applicable.

Data Availability Statement: The data presented in this study are available on request from the corresponding author.

Acknowledgments: The authors acknowledge all project partners for their support.

Conflicts of Interest: The authors declare no conflict of interest. The funders had no role in the design of the study; in the collection, analyses, or interpretation of data; in the writing of the manuscript; or in the decision to publish the results.

References

1. Xu, C.; Dai, Q.; Gaines, L.; Hu, M.; Tukker, A.; Steubing, B. Future material demand for automotive lithium-based batteries. *Commun. Mater.* **2020**, *1*, 99. [CrossRef]
2. International Energy Agency. Global Electric Vehicle Outlook 2022, Paris, 2022. Available online: https://www.iea.org/reports/global-ev-outlook-2022 (accessed on 9 July 2022).
3. *No 2019/1020*; Proposal for a Regulation of the European Parliament and of the Council Concerning Batteries and Waste Batteries, Repealing DIRECTIVE 2006/66/EC and Amending Regulation (EU). EU: Brussels, Belgium, 2020.
4. Harper, G.D.J.; Kendrick, E.; Anderson, P.A.; Mrozik, W.; Christensen, P.; Lambert, S.; Greenwood, D.; Das, P.K.; Ahmeid, M.; Milojevic, Z.; et al. Roadmap for a sustainable circular economy in lithium-ion and future battery technologies. *J. Phys. Energy* **2023**, *5*, 21501. [CrossRef]
5. Schwich, L.; Schubert, T.; Friedrich, B. Early-Stage Recovery of Lithium from Tailored Thermal Conditioned Black Mass Part I: Mobilizing Lithium via Supercritical CO_2-Carbonation. *Metals* **2021**, *11*, 177. [CrossRef]
6. Lombardo, G.; Ebin, B.; Steenari, B.-M.; Alemrajabi, M.; Karlsson, I.; Petranikova, M. Comparison of the effects of incineration, vacuum pyrolysis and dynamic pyrolysis on the composition of NMC-lithium battery cathode-material production scraps and separation of the current collector. *Resour. Conserv. Recycl.* **2021**, *164*, 105142. [CrossRef]
7. Zhang, G.; Du, Z.; He, Y.; Wang, H.; Xie, W.; Zhang, T. A Sustainable Process for the Recovery of Anode and Cathode Materials Derived from Spent Lithium-Ion Batteries. *Sustainability* **2019**, *11*, 2363. [CrossRef]
8. Vieceli, N.; Casasola, R.; Lombardo, G.; Ebin, B.; Petranikova, M. Hydrometallurgical recycling of EV lithium-ion batteries: Effects of incineration on the leaching efficiency of metals using sulfuric acid. *Waste Manag.* **2021**, *125*, 192–203. [CrossRef]
9. Stallmeister, C.; Schwich, L.; Friedrich, B. Early-Stage Li-Removal—Vermeidung von Lithiumverlusten im Zuge der Thermischen und Chemischen Recyclingrouten von Batterien. In *Recycling und Rohstoffe*; Holm, O., Thomé-Kozmiensky, E., Goldmann, D., Friedrich, B., Eds.; Thomé-Kozmiensky Verlag GmbH: Neuruppin, Germany, 2020; pp. 544–557. ISBN 978-3-944310-51-0.

10. Li, J.; Wang, G.; Xu, Z. Environmentally-friendly oxygen-free roasting/wet magnetic separation technology for in situ recycling cobalt, lithium carbonate and graphite from spent $LiCoO_2$/graphite lithium batteries. *J. Hazard. Mater.* **2016**, *302*, 97–104. [CrossRef]
11. Pinegar, H.; Smith, Y.R. Recycling of End-of-Life Lithium-Ion Batteries, Part II: Laboratory-Scale Research Developments in Mechanical, Thermal, and Leaching Treatments. *J. Sustain. Metall.* **2020**, *6*, 142–160. [CrossRef]
12. Lombardo, G.; Ebin, B.; St. Foreman, M.R.J.; Steenari, B.-M.; Petranikova, M. Chemical Transformations in Li-Ion Battery Electrode Materials by Carbothermic Reduction. *ACS Sustain. Chem. Eng.* **2019**, *7*, 13668–13679. [CrossRef]
13. Sabarny, P.; Peters, L.; Sommerfeld, M.; Stallmeister, C.; Schier, C.; Friedrich, B. Early-Stage Lithium Recovery (ESLR) for Enhancing Efficiency in Battery Recycling. In Proceedings of the AABC Europe 2020, Wiesbaden, Germany, 12–16 January 2020.
14. Rouquette, L.M.J.; Lemaître, T.; Vieceli, N.; Petranikova, M. Intensification of lithium carbonation in the thermal treatment of spent EV Li-ion batteries via waste utilization and selective recovery by water leaching. *Resour. Conserv. Recycl. Adv.* **2023**, *17*, 200125. [CrossRef]
15. Balachandran, S.; Forsberg, K.; Lemaître, T.; Vieceli, N.; Lombardo, G.; Petranikova, M. Comparative Study for Selective Lithium Recovery via Chemical Transformations during Incineration and Dynamic Pyrolysis of EV Li-Ion Batteries. *Metals* **2021**, *11*, 1240. [CrossRef]
16. Wang, J.-P.; Pyo, J.-J.; Ahn, S.-H.; Choi, D.-H.; Lee, B.-W.; Lee, D.-W. A Study on the Recovery of Li_2CO_3 from Cathode Active Material NCM($LiNiCoMnO_2$) of Spent Lithium Ion Batteries. *J. Korean Powder Metall. Inst.* **2018**, *25*, 296–301. [CrossRef]
17. Hu, J.; Zhang, J.; Li, H.; Chen, Y.; Wang, C. A promising approach for the recovery of high value-added metals from spent lithium-ion batteries. *J. Power Sources* **2017**, *351*, 192–199. [CrossRef]
18. Vishvakarma, S.; Dhawan, N. Recovery of Cobalt and Lithium Values from Discarded Li-Ion Batteries. *J. Sustain. Metall.* **2019**, *5*, 204–209. [CrossRef]
19. Xiao, J.; Li, J.; Xu, Z. Recycling metals from lithium ion battery by mechanical separation and vacuum metallurgy. *J. Hazard. Mater.* **2017**, *338*, 124–131. [CrossRef]
20. Liu, P.; Xiao, L.; Tang, Y.; Chen, Y.; Ye, L.; Zhu, Y. Study on the reduction roasting of spent $LiNixCoyMnzO_2$ lithium-ion battery cathode materials. *J. Therm. Anal. Calorim.* **2019**, *136*, 1323–1332. [CrossRef]
21. Sommerfeld, M.; Vonderstein, C.; Dertmann, C.; Klimko, J.; Oráč, D.; Miškufová, A.; Havlík, T.; Friedrich, B. A Combined Pyro- and Hydrometallurgical Approach to Recycle Pyrolyzed Lithium-Ion Battery Black Mass Part 1: Production of Lithium Concentrates in an Electric Arc Furnace. *Metals* **2020**, *10*, 1069. [CrossRef]
22. Brückner, L.; Frank, J.; Elwert, T. Industrial Recycling of Lithium-Ion Batteries—A Critical Review of Metallurgical Process Routes. *Metals* **2020**, *10*, 1107. [CrossRef]
23. Xiao, S.; Ren, G.; Xie, M.; Pan, B.; Fan, Y.; Wang, F.; Xia, X. Recovery of Valuable Metals from Spent Lithium-Ion Batteries by Smelting Reduction Process Based on MnO–SiO_2–Al_2O_3 Slag System. *J. Sustain. Metall.* **2017**, *3*, 703–710. [CrossRef]
24. Sommerfeld, M.; Hovestadt, G.; Friedrich, B. Smelting of Pyrolyzed Lithium-Ion Battery Black Mass using a Calcium-Aluminate Slag System. In Proceedings of the European Metallurgical Conference (EMC), Online, 27–30 June 2021; GDMB: Clausthal-Zellerfeld, Germany, 2021; pp. 879–902, ISBN 978-3-940276-96-4.
25. Vest, M.; Zervos, J.; Weyhe, R.; Friedrich, B. Slag Design for Lithium Recovery from Spent Batteries. Slags and Fluxes in Modern Metallurgy. In Proceedings of the International Workshop on Metal-Slag Interaction, Crimea, Ukraine, 14–19 September 2010; pp. 93–106.
26. Vest, M.; Weyhe, R.; Georgi-Maschler, T.; Friedrich, B. Rückgewinnung von Wertmetallen aus Batterieschrott. *Chem. Ing. Tech.* **2010**, *82*, 1985–1990. [CrossRef]
27. Georgi-Maschler, T.; Friedrich, B.; Weyhe, R.; Heegn, H.; Rutz, M. Development of a recycling process for Li-ion batteries. *J. Power Sources* **2012**, *207*, 173–182. [CrossRef]
28. Hu, X.; Mousa, E.; Tian, Y.; Ye, G. Recovery of Co, Ni, Mn, and Li from Li-ion batteries by smelting reduction—Part I: A laboratory-scale study. *J. Power Sources* **2021**, *483*, 228936. [CrossRef]
29. Windisch-Kern, S.; Holzer, A.; Ponak, C.; Raupenstrauch, H. Pyrometallurgical Lithium-Ion-Battery Recycling: Approach to Limiting Lithium Slagging with the InduRed Reactor Concept. *Processes* **2021**, *9*, 84. [CrossRef]
30. Stallmeister, C.; Friedrich, B. Holistic Investigation of Inert Thermal Treatment of Industrially Shredded NMC 622 Lithium-Ion Batteries and Its Influence on Selective Lithium Recovery by Water-Leaching. *Metals* **2023**. *to be published*.
31. Chen, Y.; Liu, N.; Jie, Y.; Hu, F.; Li, Y.; Wilson, B.P.; Xi, Y.; Lai, Y.; Yang, S. Toxicity Identification and Evolution Mechanism of Thermolysis-Driven Gas Emissions from Cathodes of Spent Lithium-Ion Batteries. *ACS Sustain. Chem. Eng.* **2019**, *7*, 18228–18235. [CrossRef]
32. Diaz, F.; Wang, Y.; Weyhe, R.; Friedrich, B. Gas generation measurement and evaluation during mechanical processing and thermal treatment of spent Li-ion batteries. *Waste Manag.* **2019**, *84*, 102–111. [CrossRef]
33. Park, S.; Jung, S.; Kwon, D.; Beak, M.; Kwon, E.E.; Kwon, K. Carbothermic reduction of spent Lithium-Ion batteries using CO_2 as reaction medium. *Chem. Eng. J.* **2022**, *435*, 135165. [CrossRef]
34. Schwich, L.; Friedrich, B. Environmentally Friendly Recovery of Lithium from Lithium–Sulfur Batteries. *Metals* **2022**, *12*, 1108. [CrossRef]
35. Sun, L.; Qiu, K. Vacuum pyrolysis and hydrometallurgical process for the recovery of valuable metals from spent lithium-ion batteries. *J. Hazard. Mater.* **2011**, *194*, 378–384. [CrossRef]

36. Zu, C.; Yu, H.; Li, H. Enabling the thermal stability of solid electrolyte interphase in Li-ion battery. *InfoMat* **2021**, *3*, 648–661. [CrossRef]
37. Zhu, L.; Chen, M. Development of a Two-Stage Pyrolysis Process for the End-Of-Life Nickel Cobalt Manganese Lithium Battery Recycling from Electric Vehicles. *Sustainability* **2020**, *12*, 9164. [CrossRef]
38. Diaz, F.; Flerus, B.; Nagraj, S.; Bokelmann, K.; Stauber, R.; Friedrich, B. Comparative Analysis About Degradation Mechanisms of Printed Circuit Boards (PCBs) in Slow and Fast Pyrolysis: The Influence of Heating Speed. *J. Sustain. Metall.* **2018**, *4*, 205–221. [CrossRef]
39. Vanderbruggen, A.; Sygusch, J.; Rudolph, M.; Serna-Guerrero, R. A contribution to understanding the flotation behavior of lithium metal oxides and spheroidized graphite for lithium-ion battery recycling. *Colloids Surf. A Physicochem. Eng. Asp.* **2021**, *626*, 127111. [CrossRef]
40. Mohanty, D.; Dahlberg, K.; King, D.M.; David, L.A.; Sefat, A.S.; Wood, D.L.; Daniel, C.; Dhar, S.; Mahajan, V.; Lee, M.; et al. Modification of Ni-Rich FCG NMC and NCA Cathodes by Atomic Layer Deposition: Preventing Surface Phase Transitions for High-Voltage Lithium-Ion Batteries. *Sci. Rep.* **2016**, *6*, 26532. [CrossRef]
41. Herzog, M.J.; Gauquelin, N.; Esken, D.; Verbeeck, J.; Janek, J. Facile Dry Coating Method of High-Nickel Cathode Material by Nanostructured Fumed Alumina (Al_2O_3) Improving the Performance of Lithium-Ion Batteries. *Energy Technol.* **2021**, *9*, 2100028. [CrossRef]
42. Degen, T.; Sadki, M.; Bron, E.; König, U.; Nénert, G. The HighScore suite. *Powder Diffr.* **2014**, *29*, S13–S18. [CrossRef]
43. Zhou, F.; Qu, X.; Wu, Y.; Zhao, J.; Gao, S.; Wang, D.; Yin, H. Vacuum Pyrolysis of Pine Sawdust to Recover Spent Lithium Ion Batteries: The Synergistic Effect of Carbothermic Reduction and Pyrolysis Gas Reduction. *ACS Sustain. Chem. Eng.* **2022**, *10*, 1287–1297. [CrossRef]
44. Lombardo, G.; Ebin, B.; St. Foreman, M.R.J.; Steenari, B.-M.; Petranikova, M. Incineration of EV Lithium-ion batteries as a pretreatment for recycling—Determination of the potential formation of hazardous by-products and effects on metal compounds. *J. Hazard. Mater.* **2020**, *393*, 122372. [CrossRef]
45. Freiberg, A.T.S.; Sicklinger, J.; Solchenbach, S.; Gasteiger, H.A. Li_2CO_3 decomposition in Li-ion batteries induced by the electrochemical oxidation of the electrolyte and of electrolyte impurities. *Electrochim. Acta* **2020**, *346*, 136271. [CrossRef]
46. Bale, C.W.; Bélisle, E.; Chartrand, P.; Decterov, S.A.; Eriksson, G.; Gheribi, A.E.; Hack, K.; Jung, I.H.; Kang, Y.B.; Melançon, J.; et al. FactSage Thermochemical Software and Databases, 2010–2016. *Calphad* **2016**, *26*, 189–228. [CrossRef]
47. Leisegang, T.; Meutzner, F.; Zschornak, M.; Münchgesang, W.; Schmid, R.; Nestler, T.; Eremin, R.A.; Kabanov, A.A.; Blatov, V.A.; Meyer, D.C. The Aluminum-Ion Battery: A Sustainable and Seminal Concept? *Front. Chem.* **2019**, *7*, 268. [CrossRef] [PubMed]
48. Haynes, W.M. *CRC Handbook of Chemistry and Physics: A Ready-Reference Book of Chemical and Physical Data*, 97th ed.; CRC Press: Boca Raton, FL, USA; London, UK; New York, NY, USA, 2017; ISBN 978-1-4987-5429-3.